Applied Physics Letters

RESEARCH ARTICLE | AUGUST 07 2025

# Photocurrent dynamics and carrier transport of amorphous-$Ga_2O_3$ metal–semiconductor–metal deep ultraviolet photodetectors

Yaonan Hou ; Emirhan Kutsal ; Alfred Moore ; Jonathan Evans; Huili Liang; Zengxia Mei ; Lijie Li



*Appl. Phys. Lett.* 127, 053502 (2025)
https://doi.org/10.1063/5.0285457



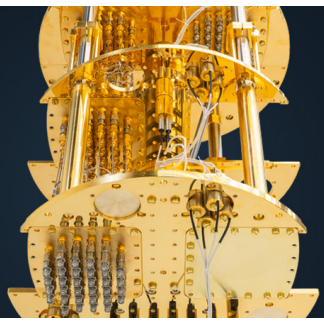

Applied Physics Letters ARTICLE pubs.aip.org/aip/apl

# Photocurrent dynamics and carrier transport of amorphous-$Ga_2O_3$ metal–semiconductor–metal deep ultraviolet photodetectors

Cite as: Appl. Phys. Lett. **127**, 053502 (2025); doi: 10.1063/5.0285457
Submitted: 15 June 2025 · Accepted: 24 July 2025 ·
Published Online: 7 August 2025



Yaonan Hou,[1,2,a] Emirhan Kutsal,[1] Alfred Moore,[2] Jonathan Evans,[2] Huili Liang,[3,4] Zengxia Mei,[3,4,b] and Lijie Li[1,2]

## AFFILIATIONS

[1]Department of Electronic and Electrical Engineering, Swansea University, Bay Campus, SA1 8EN Swansea, United Kingdom
[2]Centre for Integrative Semiconductor Materials (CISM), Swansea University, Bay Campus, SA1 8EN Swansea, United Kingdom
[3]Songshan Lake Materials Laboratory, DongGuan, Guangdong Province 523808, China
[4]Institute of Physics, Chinese Academy of Sciences, Beijing 100190, China

[a]Author to whom correspondence should be addressed: yaonan.hou@swansea.ac.uk
[b]Electronic mail: zxmei@iphy.ac.cn

## ABSTRACT

This work presents a systematic study in the photocurrent transport and transient dynamics in amorphous $Ga_2O_3$-based deep ultraviolet (DUV) photodetectors, which are configured with a co-planar metal–semiconductor–metal structure, with high performances including a DUV/dark current contrast ratio of $10^6$ and a photoresponsivity of 25.3 A/W. Under steady-state DUV excitation, an analytical current–voltage relationship is developed to describe the carrier transport behaviors. Under the pulsed-DUV excitation and post-DUV exposure, the current rise and decay dynamics have been investigated, which enables us to clarify the role of intrinsic defects in the photoresponse and response speed. In addition, we also propose a criterion to adequately evaluate the photoresponsivity of $Ga_2O_3$-based DUV photodetectors with slow photocurrent decays.





Deep ultraviolet (DUV) photodetection holds promise for various applications in healthcare, astronomy, non-line-of-sight communications, and fire warning systems.[1,2] To overcome the limitations of traditional DUV photodetectors (e.g., photomultiplier tube and Si photodiodes) including the low DUV photoresponse or the requirement of external components (e.g., spectral filters and cooling systems), extensive research in recent years has focused on DUV photodetectors fabricated from ultra-wide bandgap semiconductors, such as MgZnO, AlGaN, diamond, and $Ga_2O_3$.[3–5] Among these materials, $Ga_2O_3$ is regarded as one of the best candidates due to multiple advantages in its material properties, such as the wide bandgap energy of 4.9 eV, a tunable bandgap up to 7.6 eV by alloying with $Al_2O_3$, a large breakdown electric field of $\sim 8\ MV/cm^2$, and high chemical stability.[6] These properties endow the $Ga_2O_3$-based DUV photodetector working in Earth's atmosphere or harsh environments without losing performance.

Indeed, there has been a fast-growing interest in $Ga_2O_3$-based DUV photodetections in the past decade. Numerous metal–semiconductor–metal (MSM) photodetectors have been fabricated from single-crystal $Ga_2O_3$ with different phases (namely $a-$, $\alpha-$, $\beta-$, $\gamma-$, $\delta-$, and $\varepsilon-$ according to the crystalline structure), mainly pursuing responsivity and high sensitivity,[6–9] as well as due to the limitation of stable p-type availability.[1,6] A recent report has demonstrated an extremely large photoresponsivity of $6.7 \times 10^7$ A/W with a sensitivity of $1.06 \times 10^{21}$ Jones based on MSM structures.[10] Despite efforts made to improve response speed through vertical device designs and material innovations,[11–13] it is still unclear why large photoresponsivity is always accompanied by a slow response speed (ranging from several seconds to thousands of seconds) in such planar devices. Meanwhile, a consistent model depicting carrier transport is missing for MSM photodetectors. In this work, we demonstrated two a-$Ga_2O_3$-based MSM photodetectors with high performances, including a DUV/dark current rejection ratio of $(I_{ph}/I_{dark}) > 10^6$ and photoresponsivity up to 25.3 A/W. Through the investigation of steady-state and transient photocurrents using various testing methods, a precise current–voltage (I–V) relationship has been developed as a universal model to illustrate the carrier transport behaviors, and the defect motion coupled with

charge trapping/de-trapping process has been proposed to describe the photocurrent decay. We also point out that the *saturation photoresponsivity* should be used to appropriately evaluate the photoresponse of MSM photodetectors with slow photocurrent decay.

The undoped a-$Ga_2O_3$ thin film (150 nm) used in this work was deposited on quartz by radio frequency (RF) sputtering under oxygen (O-rich) and no-oxygen (O-deficient) conditions, where the latter contains much higher oxygen vacancy, confirmed by x-ray photoelectron spectroscopy (XPS). To be specific, both films were deposited with a $Ga_2O_3$ target under RF power of 60 W and a chamber pressure of 0.4 Pa. The O-deficient film is grown in a pure Ar environment, whilst the O-rich is one prepared in $Ar/O_2$ with an $O_2$ partial pressure of $1.6 \times 10^{-3}$ Pa. After growth, ITO interdigital electrodes were fabricated on both samples, with a finger length of 300 $\mu$m, a spacing of 5 $\mu$m, and 75 pairs. The devices were bonded to a printed circuit board with conductive silver epoxy on ITO electrodes for the electrical and optical tests. Details of the growth, XPS characterizations, and device fabrication can be found in our previous publications.[14–17] To distinguish the two devices, the photodetector fabricated on the O-rich film is labeled as device A and the one on the O-deficient film as device B. The photocurrent study was carried out with a 254 nm-DUV lamp with a Keithley 2636B source-meter with a current resolution down to 2 fA.

Figure 1(a) displays the one-loop IV measurements. Both devices show a current hysteresis with a coupled capacitance, where the detailed discussion can be found in our former publications.[18] Device B, grown in O-deficient environments, exhibits a smaller capacitance and a lower resistance. This is due to the improved conductivity as a result of the high density of oxygen vacancy, which is widely known as an n-type deep-level defect. Figure 1(b) shows the IV measured under 254 nm DUV light illumination with a sampling rate of 20 ms between each data point, where the coupled capacitance disappears in both devices due to the presence of photogenerated carriers. Typical symmetric Schottky-MSM IV curves were observed in both devices (ignoring fabrication imperfections). By considering the series resistance and the back-to-back Schottky barriers, the following equation describing the IV relationship is obtained (see details in the supplementary material):

$$V = \frac{nkT}{q} ln\left(\frac{I_0 + I}{I_0 - I}\right) + IR_s, \tag{1}$$

where k, T, and q are Boltzmann constant, temperature, and unit charge, and n, $R_s$, and $I_0$ are the ideality factor, series resistance, and reverse saturated current under DUV illumination. The data can be well fitted to Eq. (1) as shown in Fig. 1(b). It is important to note that this equation is universally valid for the Schottky-MSM structures with negligible capacitance to describe the carrier transport.

Figures 1(c) and 1(d) show the photocurrent mapping under various illumination densities. Both devices exhibit a rejection ratio ($I_{ph}/I_{dark}$) of more than 4 orders of magnitude (limited by the slow response and sampling rate in the measurement to be discussed in the later paragraphs). Device B shows that the photocurrent is more sensitive to the illumination power at high voltage as a result of improved conductivity due to oxygen vacancies, which corresponds well to the growth conditions and dark IV measurements. Although device B shows a lower photocurrent than that of device A under the same illumination density from IV measurements, it is found that the result is influenced by the device response speed and measurement sampling rate, which will be discussed later.

The photocurrent decay under different voltages was studied in order to have a deeper insight into the device working mechanism. From the results, device A shows a much faster decay than that of device B [Figs. 2(a) and 2(c)], indicating that the defects play a role. Both of the decay curves can be fitted into a multi-term exponential decay curve by

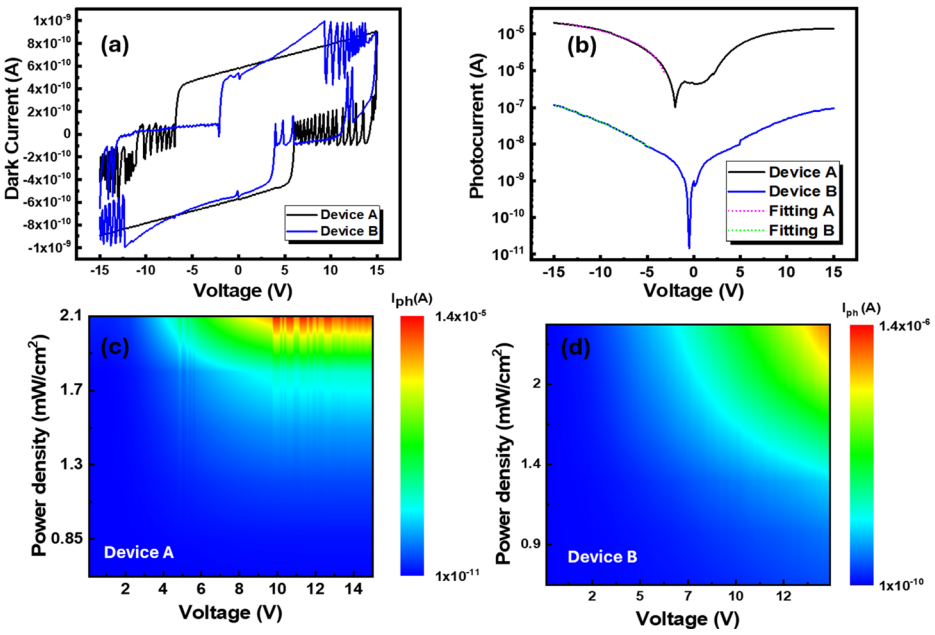


**FIG. 1.** (a) Dark current of the as-grown (device A) and annealed devices (device B). (b) The IV curve of both devices under UV254 illumination with power density of 2.1 and 3.1 mW/cm$^2$ for devices A and B. The photocurrent is limited by the sampling rate due to the long decay time. (c) and (d) Photocurrent mapping under different illumination densities of devices A and B, respectively.

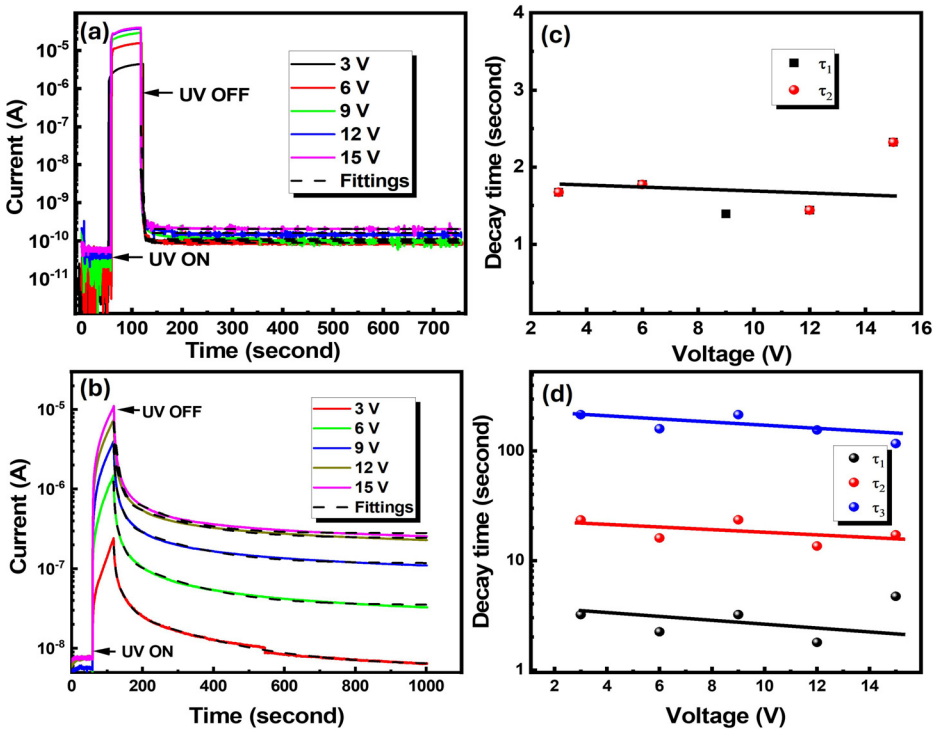


**FIG. 2.** Transient photoresponse of devices A (a) and B (c) at applied voltage from 3 to 15 V; the dashed lines are the fitting curves. (b) and (d) The time constant from the fitting of devices A and B, respectively.

$$I(t) = A\exp\left(-\frac{t}{\tau_1}\right) + B\exp\left(-\frac{t}{\tau_2}\right) + C\exp\left(-\frac{t}{\tau_3}\right), \quad (2)$$

where A, B, and C are fitting parameters; $\tau_1$, $\tau_2$, and $\tau_3$ are the decay time constants, each corresponding to a certain decay process. The decay profile of device A can be well fit into a 2-term exponential decay, while device B requires at least 3 terms to generate a good fit using Eq. (2). From the fitting results, the decay constants $\tau_1 = \tau_2$ of device A are at 1–3 s, indicating only one decay mechanism detected. In comparison, the 3 decay time constants of device B are $\tau_1 = 1$–3 s, $\tau_2 = 10$–20 s, and $\tau_3 > 100$ s [Figs. 2(b) and 2(d)]. As the fast response ($\tau_1$) in both devices is of the same value, it is rational to attribute them to the same decay process, likely to be dominated by non-radiative carrier recombination (e.g., defect-assisted recombination).[19] The medium ($\tau_2$) and slow decay ($\tau_3$) are related to carrier trapping/de-trapping and slow motion of $V_o$ and its charged defects $V_o^*$.

To verify this, the rise time of the photocurrent was measured at different voltages by turning on DUV until the photocurrent was saturated. Figures 3(a) and 3(b) are the results of the photocurrent plotted in log-scale after DUV was turned on for both devices A and B. Clearly, device A exhibits an ultra-low dark current $\sim 10$ pA under low voltage ($\leq 6$ V). With DUV illumination, the current rapidly saturates in $< 50$ s with a best $I_{ph}/I_{dark}$ ratio of $10^6$ at 6 V, among the top of the reported values.[18] The value degrades to $\sim 5$ orders when the bias is above 6 V due to the increasing dark current. Under 15 V, a maximum photoresponsivity of 0.47 A/W is observed. In device B, the large $I_{ph}/I_{dark}$ ratio of $\sim 5$ orders can be found at high voltages (e.g., 12 and 15 V), along with an exceptional photoresponsivity of 25.3 A/W. Meanwhile, the rise time of device B is much slower, where the photocurrent takes more than 200 s to achieve complete saturation. Moreover, the rise curve at low voltage (3 and 6 V) exhibits a superlinear manner [Fig. 3(c.1)], while the curve at higher voltages ($\geq 9$ V) shows a sublinear increase. Due to the complexity of the rise curve at different voltages, they hardly fit into any mathematical model. Here, we attribute the slow rise time to the presence of charged oxygen vacancies, $V^*$ (e.g., $V^+$ and $V^{2+}$). Such defects are not only electron traps but also mobile in $Ga_2O_3$ under an applied voltage.[20–22] The trapping and detrapping processes under voltage and DUV can be depicted by $V^* + e \rightleftharpoons^{\text{Voltage}}_{\text{DUV}} V_o$. Due to the existing charges, the slow-moving $V^*$ has a surrounding depleted region. As a result, the movement of other charged defects will be affected until they are neutralized by trapping electrons. Therefore, the photocurrent rise is very slow due to such a trapping process by the oxygen vacancy. Similarly, the detrapping process is also associated with the slow-moving $V^*$, which is the cause of persistent photocurrent [$\tau_3$ in Figs. 2(b) and 2(d)].

The complete relaxation of the photocurrent of device B to its initial value requires several hundred seconds [Fig. 2(b)], which is much longer than the typical sampling rate (normally $\ll 1$ s between each data point) in IV measurements. Such a situation applies to other time-related photocurrent scanning methods, e.g., spectral photoresponsivity measurements. Once the scanning rate is faster than the photocurrent decay, the obtained photocurrent (or photoresponsivity) value is not accurate, as it does not achieve the maximum value. However, this has been ignored in previous works.[5,23–25] Hence, we propose to use the *saturation photoresponsivity* measured from the photocurrent–time curve to fairly evaluate the performance of slow-decay $Ga_2O_3$-based DUV photodetectors. Figure 3(d) shows the *saturation photoresponsivity* of the two devices as a function of voltage, which can be fit to the law of the power by $R \sim V^p$. It is found that the power ($p$) of devices A and B is 0.7 (sublinear) and 3.3 (superlinear), respectively. The superlinear

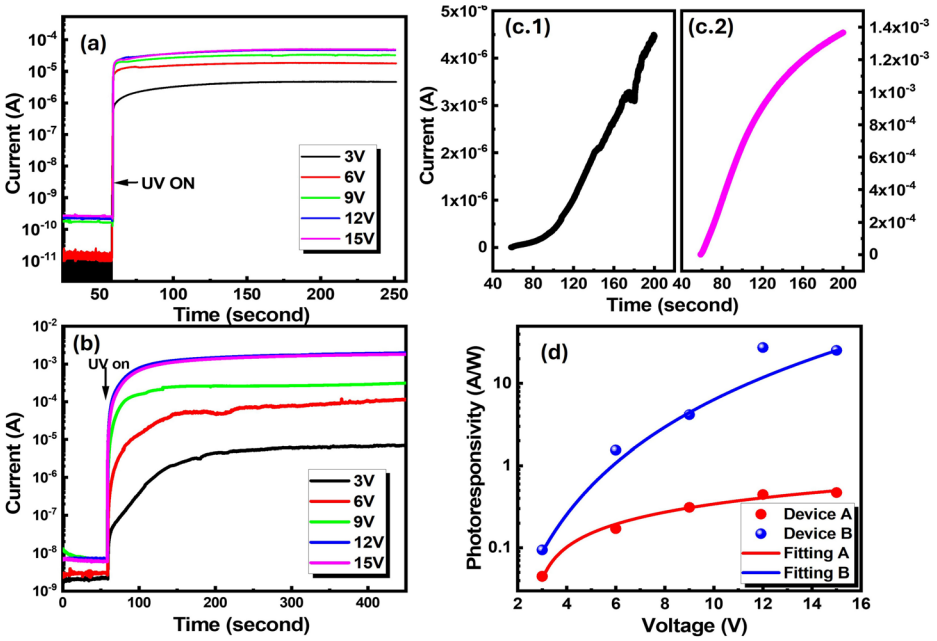


**FIG. 3.** The photocurrent rise measured under different voltages of devices A (a) and B (b), respectively. (c.1) and (c.2) show the linear plot of device B at 3 and 15 V. (d) Saturation photoresponsivity as a function of voltage for both devices.

growth of the *saturation photoresponsivity* of device B indicates a photocurrent gain, which again is related to the slow-moving $V^*$. The long lifetime of $V^*$ indicates that the charge is accumulating in the circuits, leading to the large photocurrent and gain.[26]

Finally, IV after exposing the devices to DUV ($I_{pe}$) was measured. This is different from the measurements performed in Figs. 1–3, where the IV is recorded under DUV illumination. Figures 4(a) and 4(b) show the $I_{pe}$ map under increasing DUV exposure time. Obviously, the $I_{pe}$ of device A is not relevant to DUV exposure, reflected by its value always at the dark current level [Fig. 4(a)]. In contrast, device B shows a strong increase in $I_{pe}$ over DUV exposure time [Fig. 4(b)]. The growth of $I_{pe}$ with exposure time can be fit to exponential growth,

$$I_{pe} = I_s - A\exp\left(-\frac{t}{\tau_{pe}}\right), \tag{3}$$

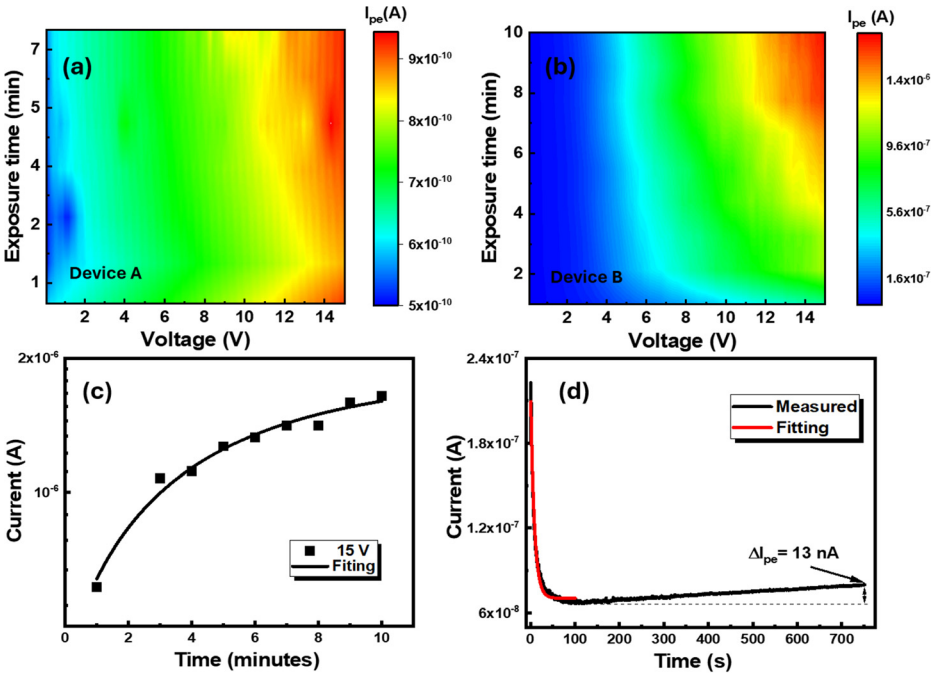


**FIG. 4.** The $I_{pe}$ mapping of devices A (a) and B (b). (c) $I_{pe}$ measured at 15 V under different DUV exposure times. (d) Transient $I_{pe}$ after 10 min DUV exposure at 3 V.

where $I_s$ is the saturated value of $I_{pe}$, and A, $\tau_{pe}$ fitting parameters. From the fitting, a saturated post-exposure current of $1.8 \times 10^{-6}$ A can be obtained at 15 V. The decay of $I_{pe}$ was measured after 10-min DUV exposure at 3 V. As shown in Fig. 4(d), the decay curve can be fitted into Eq. (2) with one-term exponential decay. The time constant ($\tau_{pe}$) is obtained with a value of 8.4 s, very close to $\tau_2 \sim 10$ s. Given that no voltage is applied during exposure, it is reasonable to conclude that this decay is dominated by the electron detrapping from $V^*$ [$\tau_2$ in Figs. 2(b) and 2(d)]. Therefore, this experiment counterproves that the long decay of $\tau_3$ is from the slow-moving charged-defect ($V^*$), where the excitation of such defects requires concomitant presence of voltage and DUV illumination. From Fig. 4(d), a slight current increase (with $\Delta I_{pe} = 13$ pA) is also observed, which could be the thermally excited carriers as a result of long-time continuous measurement. This also explains why the current is not completely relaxed to the initial value after DUV illumination in Fig. 3(a).

It is worth mentioning that the performance of our devices, including the high contrast ratio of $10^6$ and large photoresponsivity of 25.3 A/W, is amid the top of $Ga_2O_3$ DUV photodetectors, including the chemically stable $\beta$-phase ones. Detailed device performance based on various device structural designs and different crystalline phases can be found in several recent review papers.[1,6,23,27–29] One advantage of a-$Ga_2O_3$ is the simple material fabrication methods achievable at low temperature on arbitrary substrates with a low cost, enabling the application in, e.g., flexible optoelectronics.[16] Moreover, there are potentials for integrating a-$Ga_2O_3$ DUV photodetectors with its other devices such as memristors, gas sensors, and phosphors.[18,30] On the contrary, $\beta$-$Ga_2O_3$ offers superior material stability for high-power, harsh-environment applications, associated with the compatibility for accurate defect control and integration with other materials by epitaxial growth. As $Ga_2O_3$ DUV photodetection is growing rapidly, and both amorphous and $\beta$-phase (as well as other phase) materials are developing dynamically, this paper does not aim to judge which one is the final solution—this also depends on the practical application scenarios.

In summary, our work has developed a precise IV relationship for understanding the carrier transport in Schottky-MSM devices. Though the analytical equation is derived based on thermionic emission, the authors envisage that it can be further improved by considering practical carrier transport processes in wide bandgap semiconductor Schottky barriers (e.g., field emission, tunneling, and leakage). With a systematic study of the photocurrent behaviors associated with $V_o$ in a-$Ga_2O_3$, we revealed that slow decay is strongly related to the motion and electron detrapping of $V_o$ and its charged states. Moreover, we also proposed *saturation photoresponsivity* as an accurate evaluation standard of the device performance instead of traditional measurements involving spectral or photocurrent scanning, where the instantaneously obtained photocurrent may be influenced by the sampling rate in the slow response devices. Our findings in device physics are also applicable to other ultra-wide bandgap semiconductor-based MSM DUV photodetectors.

See the supplementary material for the device configuration and derivation of Eq. (1).

This work was supported by the EPSRC under Grant No. EP/T019085/1 and the Royal Society under Grant No. IEC/NSFC/242145. H.L. and Z.M. thank the support from NSFC under Grant Nos. 12174275 and 62174113.

## AUTHOR DECLARATIONS

### Conflict of Interest

The authors have no conflicts to disclose.

### Author Contributions

**Yaonan Hou:** Conceptualization (lead); Data curation (lead); Formal analysis (lead); Funding acquisition (equal); Investigation (equal); Methodology (lead); Project administration (lead); Writing – original draft (lead); Writing – review & editing (lead). **Emirhan Kutsal:** Investigation (equal); Methodology (equal); Writing – original draft (equal); Writing – review & editing (equal). **Alfred Moore:** Investigation (equal); Writing – original draft (equal); Writing – review & editing (equal). **Jonathan Evans:** Methodology (equal); Software (lead); Writing – original draft (equal); Writing – review & editing (equal). **Huili Liang:** Conceptualization (equal); Funding acquisition (equal); Investigation (equal); Methodology (equal); Writing – original draft (equal); Writing – review & editing (equal). **Zengxia Mei:** Conceptualization (equal); Funding acquisition (equal); Investigation (equal); Methodology (equal); Project administration (equal); Resources (equal); Supervision (equal); Writing – original draft (equal); Writing – review & editing (equal). **Lijie Li:** Conceptualization (equal); Funding acquisition (equal); Investigation (equal); Supervision (lead); Writing – original draft (equal); Writing – review & editing (equal).

## DATA AVAILABILITY

The data that support the findings of this study are available from the corresponding author upon reasonable request.

## REFERENCES

[1]X. Hou, Y. Zou, M. Ding, Y. Qin, Z. Zhang, X. Ma, P. Tan, S. Yu, X. Zhou, X. Zhao *et al.*, "Review of polymorphous $Ga_2O_3$ materials and their solar-blind photodetector applications," J. Phys. D **54**, 043001 (2021).
[2]H. Kurosawa, S. Tsuzuki, M. Taniguchi, and S-i Inoue, "Solar-blind optical wireless communications over 80 meters using a 265-nm high-power single-chip DUV-LED over 500 mW in sunlight," IEEE Photonics J. **15**, 7302605 (2023).
[3]Y. Hou, Z. Mei, and X. Du, "Semiconductor ultraviolet photodetectors based on ZnO and $Mg_xZn_{1-x}O$," J. Phys. D **47**, 283001 (2014).
[4]Q. Cai, H. You, H. Guo, J. Wang, B. Liu, Z. Xie, D. Chen, H. Lu, Y. Zheng, and R. Zhang, "Progress on AlGaN-based solar-blind ultraviolet photodetectors and focal plane arrays," Light: Sci. Appl. **10**, 94 (2021).
[5]H. Liang, Z. Han, and Z. Mei, "Recent progress of deep ultraviolet photodetectors using amorphous gallium oxide thin films," Phys. Status Solidi A **218**, 2000339 (2021).
[6]X. Chen, F. Ren, S. Gu, and J. Ye, "Review of gallium-oxide-based solar-blind ultraviolet photodetectors," Photonics Res. **7**, 381–415 (2019).
[7]S. Cui, Z. Mei, Y. Hou, M. Sun, Q. Chen, H. Liang, Y. Zhang, X. Bai, and X. Du, "Surface plasmon enhanced solar-blind photoresponse of $Ga_2O_3$ film with Ga nanospheres," Sci. China: Phys. Mech. Astron. **61**, 107021 (2018).
[8]Z. Han, H. Liang, W. Huo, X. Zhu, X. Du, and Z. Mei, "Boosted UV photodetection performance in chemically etched amorphous $Ga_2O_3$ thin-film transistors," Adv. Opt. Mater. **8**, 1901833 (2020).
[9]R. Zhu, H. Liang, H. Bai, T. Zhu, and Z. Mei, "Double is better: Achieving an oxide solar-blind UV detector with ultrahigh detectivity and fast-refreshing capability," Appl. Mater. Today **29**, 101556 (2022).
[10]X. Hou, C. Li, C. Chen, S. Bai, Y. Liu, Z. Peng, X. Zhao, X. Zhou, G. Xu, N. Gao, and S. Long, "High-performance $Ga_2O_3$ in-memory DUV photodetectors by

interface charge reservoir design for multifunctional applications," Adv. Mater. 2506179 (2025).
[11]Y. Wang, H. Li, J. Cao, J. Shen, Q. Zhang, Y. Yang, Z. Dong, T. Zhou, Y. Zhang, W. Tang *et al.*, "Ultrahigh gain solar blind avalanche photodetector using an amorphous $Ga_2O_3$-based heterojunction," ACS Nano **15**, 16654–16663 (2021).
[12]Y. Wang, W. Cui, J. Yu, Y. Zhi, H. Li, Z.-Y. Hu, X. Sang, E-j Guo, W. Tang, and Z. Wu, "One-step growth of amorphous/crystalline $Ga_2O_3$ phase junctions for high-performance solar-blind photodetection," ACS Appl. Mater. Interfaces **11**, 45922–45929 (2019).
[13]Y. Wang, S. Li, J. Cao, Y. Jiang, Y. Zhang, W. Tang, and Z. Wu, "Improved response speed of $\beta$-$Ga_2O_3$ solar-blind photodetectors by optimizing illumination and bias," Mater. Des. **221**, 110917 (2022).
[14]R. Zhu, H. Liang, S. Liu, Y. Yuan, X. Wang, F. C.-C. Ling, A. Kuznetsov, G. Zhang, and Z. Mei, "Non-volatile optoelectronic memory based on a photosensitive dielectric," Nat. Commun. **14**, 5396 (2023).
[15]R. Zhu, H. Liang, S. Hu, Y. Wang, and Z. Mei, "Amorphous-$Ga_2O_3$ optoelectronic synapses with ultra-low energy consumption," Adv. Electron. Mater. **8**, 2100741 (2022).
[16]H. Liang, S. Cui, R. Su, P. Guan, Y. He, L. Yang, L. Chen, Y. Zhang, Z. Mei, and X. Du, "Flexible x-ray detectors based on amorphous $Ga_2O_3$ thin films," ACS Photonics **6**, 351–359 (2019).
[17]S. Cui, Z. Mei, Y. Zhang, H. Liang, and X. Du, "Room-temperature fabricated amorphous $Ga_2O_3$ high-response-speed solar-blind photodetector on rigid and flexible substrates," Adv. Opt. Mater. **5**, 1700454 (2017).
[18]A. Moore, L. Li, H. Shao, X. Tang, H. Liang, Z. Mei, and Y. Hou, "A capacitance-coupled $Ga_2O_3$ memristor," AIP Adv. **15**, 045309 (2025).
[19]M. Labed, N. Sengouga, C. V. Prasad, M. Henini, and Y. S. Rim, "On the nature of majority and minority traps in $\beta$-$Ga_2O_3$: A review," Mater. Today Phys. **36**, 101155 (2023).
[20]Y. Aoki, C. Wiemann, V. Feyer, H.-S. Kim, C. M. Schneider, H. Ill-Yoo, and M. Martin, "Bulk mixed ion electron conduction in amorphous gallium oxide causes memristive behaviour," Nat. Commun. **5**, 3473 (2014).
[21]X. Dai, X. Zhang, D. Gong, and G. Xiang, "Performance enhancement and in situ observation of resistive switching and magnetic modulation by a tunable two-level system of Mn dopants in *a*-gallium oxide-based memristor," Adv. Funct. Mater. **33**, 2304749 (2023).
[22]K. Sato, Y. Hayashi, N. Masaoka, T. Tohei, and A. Sakai, "High-temperature operation of gallium oxide memristors up to 600 K," Sci. Rep. **13**, 1261 (2023).
[23]Y. Qin, S. Long, H. Dong, Q. He, G. Jian, Y. Zhang, X. Hou, P. Tan, Z. Zhang, H. Lv *et al.*, "Review of deep ultraviolet photodetector based on gallium oxide," Chin. Phys. B **28**, 018501 (2019).
[24]A. Singh Pratiyush, S. Krishnamoorthy, S. Vishnu Solanke, Z. Xia, R. Muralidharan, S. Rajan, and D. N. Nath, "High responsivity in molecular beam epitaxy grown $\beta$-$Ga_2O_3$ metal semiconductor metal solar blind deep-UV photodetector," Appl. Phys. Lett. **110**, 221107 (2017).
[25]L. Qian, H. Liu, H. Zhang, Z. Wu, and W. Zhang, "Simultaneously improved sensitivity and response speed of $\beta$-$Ga_2O_3$ solar-blind photodetector via localized tuning of oxygen deficiency," Appl. Phys. Lett. **114**, 113506 (2019).
[26]S. Han, Z. Zhang, J. Zhang, L. Wang, J. Zheng, H. Zhao, Y. Zhang, M. Jiang, S. Wang, D. Zhao *et al.*, "Photoconductive gain in solar-blind ultraviolet photodetector based on $Mg_{0.52}Zn_{0.48}O$ thin film," Appl. Phys. Lett. **99**, 242105 (2011).
[27]W. Wu, H. Huang, Y. Wang, H. Yin, K. Han, X. Zhao, X. Feng, Y. Zeng, Y. Zou, X. Hou *et al.*, "Structure engineering of $Ga_2O_3$ photodetectors: A review," J. Phys. D **58**, 063003 (2024).
[28]A. Moore, S. Rafique, C. Llewelyn, D. Lamb, and L. Li, "A review of $Ga_2O_3$ heterojunctions for deep-UV photodetection: Current progress, methodologies, and challenges," Adv. Electron. Mater. **11**, 2400898 (2025).
[29]D. Guo, Q. Guo, Z. Chen, Z. Wu, P. Li, and W. Tang, "Review of $Ga_2O_3$-based optoelectronic devices," Mater. Today Phys. **11**, 100157 (2019).
[30]Z.-Y. Xi, L.-L. Yang, L.-C. Shu, M.-L. Zhang, S. Li, L. Shi, Z. Liu, Y.-F. Guo, and W.-H. Tang, "The growth and expansive applications of amorphous $Ga_2O_3$," Chin. Phys. B **32**, 088502 (2023).